ADVANCED MATERIALS
www.advmat.de

Unexpected Crystal and Domain Structures and Properties in Compositionally Graded $PbZr_{1-x}Ti_xO_3$ Thin Films

*R. V. K. Mangalam, J. Karthik, Anoop R. Damodaran, Joshua C. Agar, and Lane W. Martin**

Ferroelectric thin films and heterostructures have been widely investigated as functional elements for a variety of applications.[1–4] The interest in these materials is due primarily to the presence of a strong spontaneous polarization and large dielectric, piezoelectric, and pyroelectric susceptibilities.[3,4] In bulk versions of these materials (i.e., single crystals or sintered ceramics), researchers have primarily varied the chemical composition as a means to control these susceptibilities.[5,6] In this spirit, the lead zirconate titanate, $PbZr_{1-x}Ti_xO_3$ (PZT), family of materials has been widely studied because strong chemically driven phase competition in this material gives rise to large susceptibilities. Separating the two structural polymorphs of the PZT system (a tetragonal phase on the Ti-rich side and a rhombohedral phase on the Zr-rich side) is a nearly temperature independent, compositionally driven boundary called a morphotropic phase boundary (MPB) (occurring at $x = 0.48$).[5,7] Additionally, advances in thin-film epitaxy over the last decade have also provided added routes by which to control properties in these materials including utiliztion of epitaxial strain,[8] film thickness, electrical boundary conditions,[9] creation of complex bilayer and superlattice heterostructures,[10–14] and much more. In PZT, for instance, bilayer films give rise to large dielectric and piezoelectric properties[10] and superlattices have been utilized to obtain exquisite control over spontaneous polarization, dielectric constant, and Curie temperature.[13,15]

Likewise, compositionally graded thin films, which possess a smooth variation in the composition throughout the thickness of the film, have shown considerable promise. Compositional gradients have been utilized in semiconductor epitaxy (in systems such as Si_xGe_{1-x} and $In_{1-x}Ga_xAs$) to engineer strain for the growth of dislocation-free epilayers and for bandgap control.[16–18] In the realm of ferroelectrics, prior work on compositionally graded ferroelectric thin films of a variety of systems including PZT and $Ba_{1-x}Sr_xTiO_3$ has revealed a range of novel phenomena such as the presence of built-in electric fields,[19] shifted hysteresis loops,[19–22] and large susceptibilities.[23] Recent theoretical work has suggested that compositionally graded thin films could have signatures of geometric frustration[24] and experimental efforts have explored flexoelectric effects assoicated with strain gradients[25,26] that could also be important in compositionally graded films. Despite a longstanding scientific interest and an immense potential for applications, the origin of the novel properties and the structure-property relationships in compositionally graded films is still unclear. In turn, this has limited the adoption and utilization of these graded materials as compared to more traditional epitaxial strain approaches to engineer and control functionality in thin-film ferroelectrics.

Here, we report on the evolution of structural, dielectric, and ferroelectric properties in single-layer, bilayer, and compositionally graded PZT films. We observe that both bilayer and compositionally graded heterostructures have ferroelectric domain structures that are largely determined by the structural evolution at the film-substrate interface. By minimizing the lattice misfit at the interface, large residual strains can be generated in the heterostructures which gives rise to exotic ferroelectric domain structures that are not found in single layer versions of these materials. Correspondingly, novel dielectric and ferroelectric properties including the observation of built-in electric fields and two different zero-field stable states with the same net polarization, but different small-signal dielectric permittivity have been observed. In the remainder of this work, we will provide a detailed framework by which to understand the complex evolution of structure and properties in this system and identify potential avenues for future applications.

We focus our attention on 100 nm thick films of PZT with compositions between x = 0.2–0.8. The two end-members are $PbZr_{0.2}Ti_{0.8}O_3$ (a tetragonal ferroelectric with lattice parameters $a = 3.94$ Å and $c = 4.12$ Å)[27] and $PbZr_{0.8}Ti_{0.2}O_3$ (a rhombohedral ferroelectric with lattice parameter $a = 4.118$ Å and $\alpha = 89.73°$).[28] Considering the bulk lattice parameters of $PbZr_{0.2}Ti_{0.8}O_3$ and $PbZr_{0.8}Ti_{0.2}O_3$, $GdScO_3$ (110) single crystal substrates (with a pseudocubic lattice parameter a_{pc} = 3.973 Å that is between the two phases) are used for this study. Six variants of heterostructures were studied: 1) single-layer $PbZr_{0.2}Ti_{0.8}O_3$ (**Figure 1**a); 2) single-layer $PbZr_{0.8}Ti_{0.2}O_3$ (Figure 1b); 3) up-bilayer heterostructures (a 50 nm $PbZr_{0.8}Ti_{0.2}O_3$ layer grown on a 50 nm layer of $PbZr_{0.2}Ti_{0.8}O_3$) (Figure 1c); 4) down-bilayer heterostructures (a 50 nm $PbZr_{0.2}Ti_{0.8}O_3$ film grown on a 50 nm layer of $PbZr_{0.8}Ti_{0.2}O_3$) (Figure 1d); 5) compositionally up-graded heterostructures (which smoothly transition from $PbZr_{0.2}Ti_{0.8}O_3$ to $PbZr_{0.8}Ti_{0.2}O_3$ from the substrate to the film surface) (Figure 1e); and 6) compositionally down-graded heterostructures (which smoothly transition from $PbZr_{0.8}Ti_{0.2}O_3$ to $PbZr_{0.2}Ti_{0.8}O_3$ from the substrate to the film surface) (Figure 1f). In all cases, the PZT heterostructures are grown with a 30 nm $SrRuO_3$ bottom

Dr. R. V. K. Mangalam, J. Karthik, A. R. Damodaran, J. C. Agar, Prof. L. W. Martin
Department of Materials Science and Engineering and Materials Research Laboratory
University of Illinois
Urbana-Champaign, Urbana, IL 61801, USA
E-mail: lwmartin@illinois.edu

DOI: 10.1002/adma.201204240

© 2013 WILEY-VCH Verlag GmbH & Co. KGaA, Weinheim

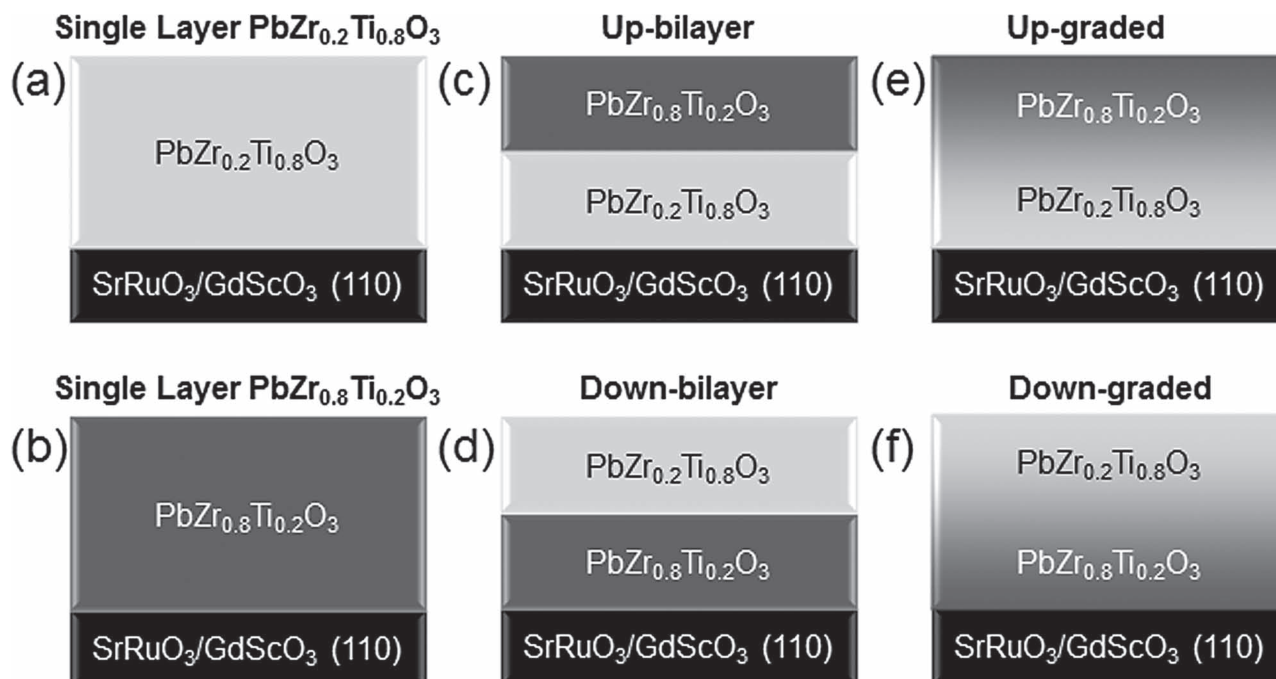

Figure 1. Schematic illustrations of the six sample variants studied in this work including: a) single-layer $PbZr_{0.2}Ti_{0.8}O_3$, b) single-layer $PbZr_{0.8}Ti_{0.2}O_3$, c) up-bilayer, d) down-bilayer, e) up-graded, and f) down-graded heterostructures.

electrode. Additional details of the growth are provided in the Experimental Section. The variation in composition across the thickness of the film was confirmed using time-of-flight secondary ion mass spectrometry (TOF-SIMS) analysis with both single-layer $PbZr_{0.2}Ti_{0.8}O_3$ (**Figure 2**a) and $PbZr_{0.8}Ti_{0.2}O_3$ (Figure 2b) films revealing essentially constant Zr and Ti ion concentrations across the thickness of the films and compositionally graded samples revealing a gradual change in the Zr and Ti ion concentration across the thickness of the films (Figure 2c,d). Note that in TOF-SIMS analysis ion signals can only be related to the composition of the bulk of the material (typically >10 nm) where the ion yield transients arising from surface contaminants are reduced and the implantation of the primary beam species produces a steady-state level of the species.[29] The TOF-SIMS analysis reported here is meant simply to confirm that the compositionally graded variants have smoothly varying Zr- and Ti-contents across the thickness of the film.

The structure of these heterostructures was studied using X-ray diffraction reciprocal space mapping (RSM) about the 103 and 332 diffraction conditions for the film and substrate, respectively. These studies reveal that single-layer $PbZr_{0.2}Ti_{0.8}O_3$ films are coherently strained to the $GdScO_3$ (110) substrates (Figure 2e) while single-layer $PbZr_{0.8}Ti_{0.2}O_3$ films are partially relaxed (Figure 2f). We observe a similar asymmetry in strain relaxation in the bilayer heterostructures where the up-bilayer variants possess a majority tetragonal-like structure with some indication of partial strain relaxation (Figure 2g) while the down-bilayer variants possess peaks for both the rhombohedral ($PbZr_{0.8}Ti_{0.2}O_3$, referred to as PZT_R in the Figure) and tetragonal ($PbZr_{0.2}Ti_{0.8}O_3$, referred to as PZT_T in the Figure) phases including evidence of in-plane *a* domain formation in the $PbZr_{0.2}Ti_{0.8}O_3$ and complete strain relaxation (Figure 2h). Furthermore, in the compositionally graded heterostructures the up-graded variants are found to possess a nearly coherently-strained tetragonal-like structure with lattice parameters a = 3.973 Å and c = 4.136 Å (Figure 2i) while the down-graded variants exhibit peaks corresponding to relaxed versions of the rhombohedral phase and *a* domains of the tetragonal phase (Figure 2j).

The asymmetry in the strain relaxation and the observed crystal structures is fairly straightforward to understand. Recall that the lattice mismatch between $PbZr_{0.2}Ti_{0.8}O_3$ and the substrate (0.8% tensile) is considerably smaller than the lattice mismatch between the $PbZr_{0.8}Ti_{0.2}O_3$ and the substrate (3.5% compressive). As a result, the 100 nm thick films of $PbZr_{0.8}Ti_{0.2}O_3$ are more susceptible to strain relaxation as compared to $PbZr_{0.2}Ti_{0.8}O_3$ films of the same thickness. Therefore, the down-bilayer and down-graded variants are expected to undergo rapid strain relaxation and present the subsequent Ti-rich phase with an effectively larger in-plane lattice parameter than the $GdScO_3$ substrate. The Ti-rich (tetragonal) material will, in turn, accommodate the large tensile strain via the formation of *a* domains. This is consistent with the observed diffraction patterns in down-bilayer (Figure 2h) and down-graded (Figure 2j) variants. On the other hand, when the Ti-rich material is grown at the substrate interface, the small lattice mismatch with the substrate is easily accommodated and the subsequent Zr-rich material is presented with in-plane lattice parameters that are more favorable for generating a compressively strained variety of the Zr-rich phases. In this case, akin to what has been observed in graded semiconductor heterostructures, large strains can be achieved across the film thickness because locally the lattice mismatch throughout the film is considerably smaller.

© 2013 WILEY-VCH Verlag GmbH & Co. KGaA, Weinheim

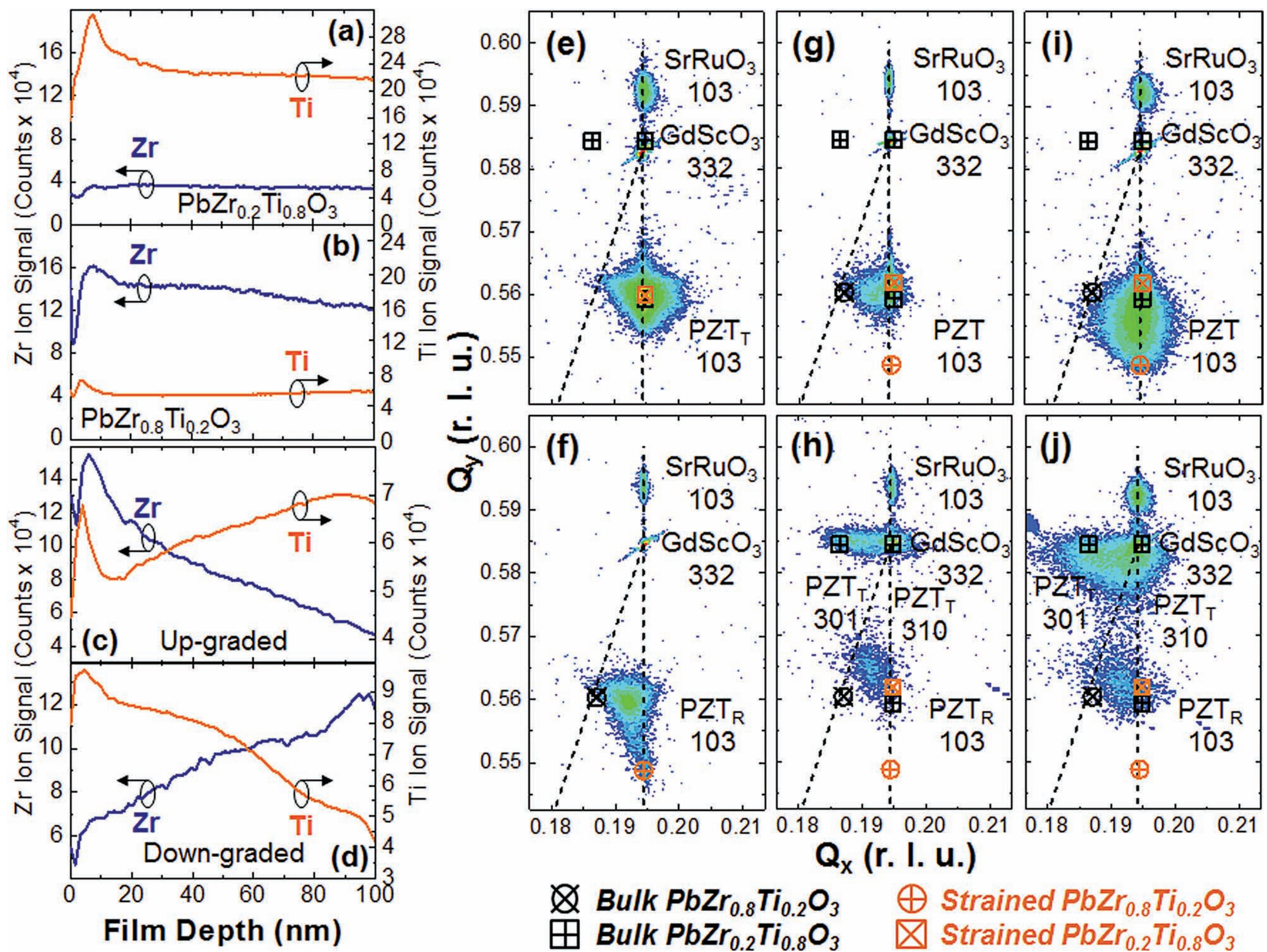

Figure 2. Time-of-flight secondary-ion mass spectra for single-layer (a) $PbZr_{0.2}Ti_{0.8}O_3$ and (b) $PbZr_{0.8}Ti_{0.2}O_3$ and compositionally (c) up-graded and (d) down-graded variants. Reciprocal-space mapping about the 103 and 332-diffraction conditions for: (e) single-layer $PbZr_{0.2}Ti_{0.8}O_3$, (f) single-layer $PbZr_{0.8}Ti_{0.2}O_3$, (g) up-bilayer, (h) down-bilayer, (i) up-graded, and (j) down-graded variants. Expected peak positions for bulk (black) and strained (orange) versions of the parent phases are labeled in each graph. Note that when appropriate and distinct, we distinguish between peaks arising from Zr-rich and Ti-rich $PbZr_{1-x}Ti_xO_3$ as PZT_R and PZT_T, respectively.

These observations are further supported by imaging the ferroelectric domain structure of these variants using piezoresponse force microscopy (PFM). A full set of phase and amplitude images is provided for each of the six sample variants in Figure S1 of the Supporting Information, but for brevity, we show here (**Figure 3**) only a sub-set to highlight the differences in domain structure between the variants. Analysis of the single-layer $PbZr_{0.2}Ti_{0.8}O_3$ variants (Figure 3a) confirms the presence of out-of-plane (*c*) and in-plane (*a*) polarized domains consistent with the 90° domain structures typically observed in such tetragonal ferroelectrics.[30–32] The single-layer $PbZr_{0.8}Ti_{0.2}O_3$ variants, however, display a much more complex domain structure (Figure 3b). Up-bilayer variants (Figure 3c) (with $PbZr_{0.8}Ti_{0.2}O_3$ at the top of the film) display a complex domain structure similar to the single-layer $PbZr_{0.8}Ti_{0.2}O_3$ variants while the down-bilayer variants (Figure 3d) reveal the presence of a_1 and a_2 domains consistent with a tensile strained Ti-rich (tetragonal) phase. Finally, the up-graded variants exhibit domain structures consisting of *c* and *a* domains (generally found in Ti-rich, tetragonal phases of PZT) (Figure 3e) despite the fact that the top 50 nm of this heterostructure is made up of Zr-rich (rhombohedral) phases. On the other hand, the down-graded variants exhibit a domain structure much like that in the down-bilayer variants where there are a_1 and a_2 domains as expected from a tensile strained Ti-rich (tetragonal) phase (Figure 3f).

Both the RSMs and the PFM images confirm an unexpected observation: the ability to produce a tetragonal-like version of Zr-rich PZT. Such a tetragonal variant of the parent rhombohedral compositions has been predicted previously[33] but was thought to be challenging to obtain due to the difficulty in retaining such large strains in thin films. It appears, however, that compositional gradients can be used to dramatically extend the range of strain (similar to the approaches used in traditional group IV and III–V semiconductors) and thereby enable Zr-rich phases to be strained considerably more than is possible in a

© 2013 WILEY-VCH Verlag GmbH & Co. KGaA, Weinheim

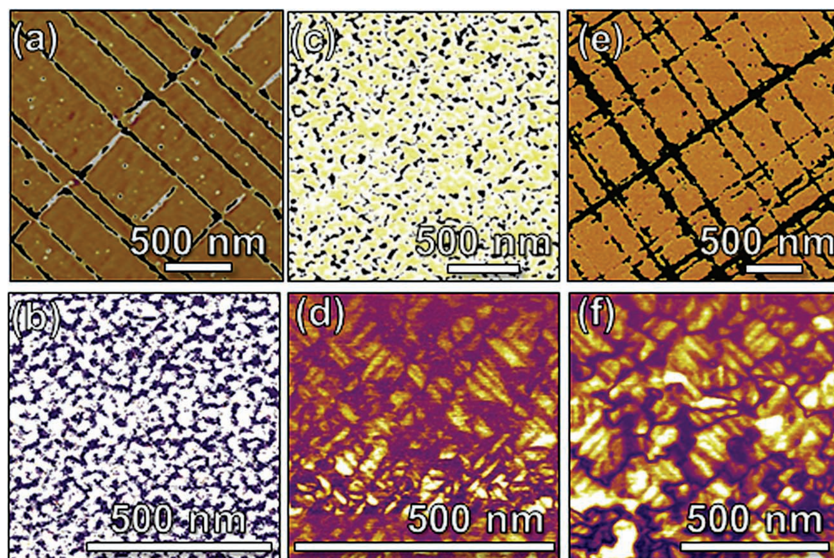

Figure 3. Piezoresponse force microscopy images of: a) single-layer $PbZr_{0.2}Ti_{0.8}O_3$ (vertical phase), b) single-layer $PbZr_{0.8}Ti_{0.2}O_3$ (vertical phase), c) up-bilayer (vertical phase), d) down-bilayer (lateral amplitude), e) up-graded (vertical phase), and f) down-graded (lateral amplitude) variants.

single layer film. These studies suggest that the ultimate structure of the bilayer and compositionally graded heterostructures is determined by the initial phase that grows thereby producing an asymmetry in the observed structures.

We proceeded to probe the impact of this complex structural evolution on the dielectric and ferroelectric properties at room temperature. Symmetric capacitor structures (circular capacitors, diameter 25–100 μm) with $SrRuO_3$ electrodes were fabricated using an MgO-based hard-mask process.[34] Capacitance–voltage and polarization-electric-field studies were performed as a function of frequency and excitation voltage to compare the response across the different heterostructures. For all data reported here, the bottom electrode was connected to ground and the drive voltage was applied to the top electrode.

We begin with studies of ferroelectric hysteresis in the materials. The hysteresis loops for all six sample variants were measured at a range of frequencies, but for brevity, loops acquired at 1 kHz are provided (**Figure 4**). Two distinct behaviors were observed; that for down-bilayer and down-graded and that for up-bilayer and up-graded variants. Let us begin with the down-bilayer and down-graded variants (Figure 4a) which both show symmetric hysteresis loops with greatly diminished remnant and saturation polarization compared to single-layer films of both $PbZr_{0.2}Ti_{0.8}O_3$ and $PbZr_{0.8}Ti_{0.2}O_3$. This is likely explained by the fact that both variants possess a large fraction of in-plane polarized *a* domains in the tetragonal phase (which cannot be switched to be out-of-plane polarized) and thus nearly half of the film is essentially ferroelectrically inactive in this device geometry. The up-bilayer and up-graded variants, on the other hand, show very different behavior (Figure 4b) with significantly shifted (along the field axis) hysteresis loops and large saturation and remnant polarization (commensurate with that measured in the single-layer films). In the case of the up-bilayer and up-graded variants, the stabilization of tetragonal-like structures means that the entire thickness of the film can produce switchable polarization (thus the large saturation and remnant polarization). More interestingly, the up-bilayer and (more so) the up-graded variants show large horizontal shifts of the hysteresis loops (along the electric field axis) of up to ≈200 kV/cm that are not observed in any of the other sample variants. We note that by reversing the polarity of the hysteresis measurements (i.e., with the drive-voltage applied to the bottom electrode and the top electrode grounded) we observed that the hysteresis loop was shifted in the opposite direction (Supporting Information, Figure S2). Although reminiscent of an imprint,[4] which can occur due to a variety of extrinsic factors such as space charge accumulation due to asymmetric electrodes or the presence of defect dipoles within the ferroelectric,[35,36] the observed shifts of the hysteresis loop are indeed intrinsic to the sample. Classic imprint can be easily eliminated with symmetric capacitor structures and oxide electrodes (such as the $SrRuO_3$ electrodes used here) and the fact that only the up-bilayer and up-graded variants show the shift indicates a different driving force for this effect. Prior work on single-layer thin

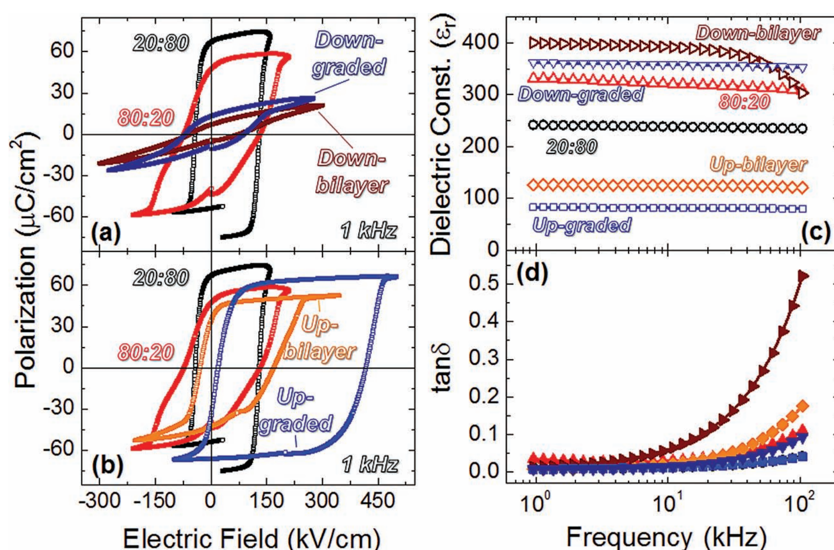

Figure 4. Room temperature, 1 kHz polarization-electric field hysteresis loops for: a) down-bilayer and -graded variants, and b) up-bilayer and -graded variants. c) Dielectric permittivity and d) loss tangent for each of the six sample variants as a function of frequency.

© 2013 WILEY-VCH Verlag GmbH & Co. KGaA, Weinheim

films, however, has highlighted the role of strain gradients (or flexoelectricity) within the film as a possible mechanism for the formation of a built-in electric field.[37–39] Our structural studies have revealed significant retention of compressive strain in the up-graded variant resulting in strain gradients as large as 4.3×10^5 m^{-1} (corresponding to a 4.3% strain gradient over a 100 nm thick film) which could be responsible for the observed voltage offsets. In this case, the gradient in composition naturally leads to a gradient in strain and provides for the generation of the built-in electric field.

The observed built-in electric fields also have a large effect on the small signal dielectric permittivity (ε) of the heterostructures (details in Experimental Section). Detailed Rayleigh behavior studies (Supporting Information, Figure S3) were used to determine the measurement voltage and confirm the absence of irreversible contributions to the permittivity. The frequency-dependent permittivity falls into three distinct regimes. The single-layer $PbZr_{0.8}Ti_{0.2}O_3$, the down-bilayer, and the down-graded variants exhibit permittivity values in excess of 300 across all frequencies studied (Figure 4c) which is consistent with what is expected for samples possessing polydomain structures and large extrinsic contribution from domain walls.[32] The single-layer $PbZr_{0.2}Ti_{0.8}O_3$ variants show intermediate permittivity with a value around 250 across all frequencies studied. This is consistent with the value reported in polydomain films with similar domain structures.[32] Finally, the up-bilayer and up-graded variants exhibit considerably reduced permittivity between 80–120 at all frequencies studied. This is comparable to the intrinsic dielectric constant of single-domain PZT.[40] It has been shown previously that inhomogeneous strain or strain gradients can lead to significant reduction in dielectric permittivity.[37–39] Our studies confirm this observation exactly with the variants exhibiting the lowest permittivity corresponding to those variants observed to have the largest strain gradients. These prior studies, however, do not comment on the microscopic mechanism giving rise to reduced dielectric response. We contend that the presence of built-in fields can reduce the extrinsic contribution from domain walls due to an effective stiffening or pinning of the domain walls due to the increased stability of a single polarization variant at zero bias. In other words, the presence of a built-in potential pointing parallel to the *c* domains of these heterostructures, could potentially skew the energy landscape such that the small signal susceptibility is greatly diminished. We have further extracted values of the Rayleigh coefficient for each sample variant which supports these observations (**Table 1**). The Rayleigh coefficient is a quantitative measurement of the irreversible domain wall contribution to the permittivity. We observe larger Rayleigh coefficients for single-layer $PbZr_{0.8}Ti_{0.2}O_3$, down-bilayer, and down-graded variants as compared to up-bilayer and up-graded variants suggesting that domain wall motion in the later variants is suppressed and could be playing a role in decreasing the overall permittivity of the samples.

Finally, we have explored permittivity (or capacitance)–voltage butterfly loops for all sample variants. Interesting differences were observed between sample variants that do and do not exhibit built-in electric fields in the ferroelectric hysteresis loops. For example, the up-graded variants (**Figure 5**a) exhibit two distinct small-signal permittivity values and asymmetric butterfly loop shape whereas down-graded variants (Figure 5b) exhibit only a single value of small-signal permittivity and a symmetric loop shape. This is an interesting observation and could have potential for new modalities of operation for non-volatile, low-power memories. Unlike traditional ferroelectric memories which require multiple capacitors to store a single data bit and destructive read/write operations, a new configuration based on the measurement of zero-bias capacitance would offer smaller feature size and non-destructive read operations. Additionally, other applications (e.g., piezoelectric vibrational energy scavenging) that require a constant and known polarization direction to enable repeatable and consistent device operation could utilize such materials. In particular, to improve the performance of a material in piezoelectric vibrational energy scavenging applications, one needs a material which simultaneously exhibits large piezoelectric response, low dielectric constant, and improved robustness to depolarization/aging. Traditionally this has been achieved in ferroelectrics by utilizing imprint or built-in electric fields that arise from the use of asymmetric electrodes.[2] The use of compositionally graded materials could provide a new pathway to improved performance in each of these areas.

Table 1. Rayleigh coefficient for each of the six sample variants.

Heterostructure	α' [cm/kV]
20:80	1.40
80:20	2.06
Up-bilayer	0.33
Down-bilayer	1.87
Up-graded	0.28
Down-graded	0.59

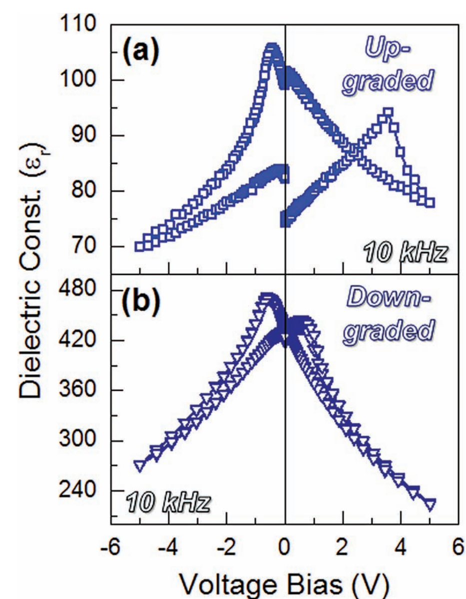

Figure 5. Room-temperature dielectric permittivity–voltage butterfly loops of compositionally (a) up-graded and (b) down-graded variants.

© 2013 WILEY-VCH Verlag GmbH & Co. KGaA, Weinheim

In summary, bilayer and compositionally graded PZT variants have been observed to possess exotic structural and ferroelectric properties that are largely determined by the structure of the initial growth layer. We have observed that up-bilayer and up-graded variants exhibit nearly coherently strained, tetragonal-like crystal and ferroelectric domain structures despite having large fractions of the film with compositions on the rhombohedral side of the phase diagram. Analogous to prior work in traditional semiconductor systems, the compositional grading of the film gives rise to a gradual increase in the magnitude of strain from the substrate and a reduced susceptibility to strain relaxation. This results in heterostructures which possess ferroelectric hysteresis loops with large voltage offsets, large remnant polarization, and low permittivity compared to other sample variants. Composition and strain gradients are, in turn, demonstrated as a powerful new tool to tune the properties of ferroelectric thin films and further evolution of this concept could represent a new direction in epitaxial thin film manipulation of complex oxide materials.

Experimental Section

Single-layer, bilayer, and compositionally-graded heterostructures of total thickness 100 nm were synthesized on 30 nm $SrRuO_3$ bottom electrode layers on single crystal $GdScO_3$ (110) substrates via pulsed-laser deposition from $Pb_{1.1}Zr_{0.2}Ti_{0.8}O_3$ and $Pb_{1.1}Zr_{0.8}Ti_{0.2}O_3$ targets. The laser fluence and repetition rate were maintained at 1.9 J/cm^2 and 3 Hz for all PZT growths and 1.8 J/cm^2 and 13 Hz for the growth of the $SrRuO_3$. Compositionally graded heterostructures were synthesized by continuously varying the composition from $PbZr_{0.2}Ti_{0.8}O_3$ to $PbZr_{0.8}Ti_{0.2}O_3$ and vice versa using a programmable target rotator (Neocera, LLC) that was synced with our excimer laser. The up-bilayer and compositionally up-graded heterostructures were grown at 600 °C. The down-bilayer and compositionally down-graded heterostructures were grown at 560 °C. For all the samples, films were grown at oxygen pressures of 200 mTorr and were cooled in 700 Torr pressure of oxygen. Capacitor structures were fabricated using 30 nm $SrRuO_3$ bottom electrodes and 80 nm $SrRuO_3$ top electrodes.

The dielectric permittivity was extracted from the measured capacitance (C) using $C = \frac{\varepsilon_0 \varepsilon_r A}{d}$ where A is the area of the capacitor and d is the thickness of the film. Prior to measurement, the films were poled with a negative bias for 0.1 milliseconds and films were measured at remanence. The dielectric permittivity as a function of frequency was measured with a tickle voltage of 8 mV (rms) and for the case of dielectric permittivity–voltage butterfly loops, the measurements were done with a tickle voltage of 8 mV (rms) at 10 kHz.

Supporting Information

Supporting Information is available from the Wiley Online Library or from the author.

Acknowledgements

The authors would like to acknowledge Dr. T. Spila at the Center for Microanalysis of Materials at UIUC for help with ToF SIMS measurements and Dr. S. Burdin for help with surface profilometer analysis. R.V.K.M. and L.W.M. acknowledge the support of the Defense Advanced Research Projects Agency (DARPA) under grant number N66001-11-1-4195. J.K. and L.W.M. acknowledge support from the Office of Naval Research under grant number N00014-10-10525. A.R.D. and L.W.M. acknowledge support from the Army Research Office under grant W911NF-10-1-0482. J.A. and L.W.M. acknowledge support from the Air Force Office of Scientific Research under grant AF FA 9550-11-1-0073. Experiments were carried out in part in the Materials Research Laboratory Central Facilities, University of Illinois, Urbana-Champaign.

Received: October 10, 2012
Revised: November 25, 2012
Published online: January 29, 2013

[1] J. F. Scott, *Science* **2007**, *315*, 954.
[2] S. H. Baek, J. Park, D. M. Kim, V. A. Aksyuk, R. R. Das, S. D. Bu, D. A. Felker, J. Lettieri, V. Vaithyanathan, S. S. N. Bharadwaja, N. Bassiri-Gharb, Y. B. Chen, H. P. Sun, C. M. Folkman, H. W. Jang, D. J. Kreft, S. K. Streiffer, R. Ramesh, X. Q. Pan, S. Trolier-McKinstry, D. G. Schlom, M. S. Rzchowski, R. H. Blick, C. B. Eom, *Science* **2011**, *334*, 958.
[3] M. Dawber, K. M. Rabe, J. F. Scott, *Rev. Mod. Phys.* **2005**, *77*, 1083.
[4] N. Setter, D. Damjanovic, L. Eng, G. Fox, S. Gevorgian, S. Hong, A. Kingon, H. Kohlstedt, N. Y. Park, G. B. Stephenson, I. Stolitchnov, A. K. Taganstev, D. V. Taylor, T. Yamada, S. Streiffer, *J. Appl. Phys.* **2006**, *100*, 051606.
[5] E. Cross, *Nature* **2004**, *432*, 24.
[6] B. Jaffe, R. S. Roth, S. Marzullo, *J. Appl. Phys.* **1954**, *25*, 809.
[7] B. Noheda, D. E. Cox, G. Shirane, J. A. Gonzalo, L. E. Cross, S. E. Park, *Appl. Phys. Lett.* **1999**, *74*, 2059.
[8] D. G. Schlom, L.-Q. Chen, C.-B. Eom, K. M. Rabe, S. K. Streiffer, J.-M. Triscone, *Annu. Rev. Mater. Res.* **2007**, *37*, 589.
[9] L. W. Martin, Y. H. Chu, R. Ramesh, *Mater. Sci. Eng. R.* **2010**, *68*, 89.
[10] V. Anbusathaiah, D. Kan, F. C. Kartawidjaja, R. Mahjoub, M. A. Arredondo, S. Wicks, I. Takeuchi, J. Wang, V. Nagarajan, *Adv. Mater.* **2009**, *21*, 3497.
[11] H. Zheng, J. Wang, S. E. Lofland, Z. Ma, L. Mohaddes-Ardabili, T. Zhao, L. Salamanca-Riba, S. R. Shinde, S. B. Ogale, F. Bai, D. Viehland, Y. Jia, D. G. Schlom, M. Wuttig, A. Roytburd, R. Ramesh, *Science* **2004**, *303*, 661.
[12] M. Dawber, C. Lichtensteiger, M. Cantoni, M. Veithen, P. Ghosez, K. Johnston, K. M. Rabe, J. M. Triscone, *Phys. Rev. Lett.* **2005**, *95*, 177601.
[13] M. Dawber, N. Stucki, C. Lichtensteiger, S. Gariglio, P. Ghosez, J. M. Triscone, *Adv. Mater.* **2007**, *19*, 4153.
[14] E. Bousquet, M. Dawber, N. Stucki, C. Lichtensteiger, P. Hermet, S. Gariglio, J.-M. Triscone, P. Ghosez, *Nature* **2008**, *452*, 732.
[15] I. Vrejoiu, M. Alexe, D. Hesse, U. Gösele, *Adv. Funct. Mater.* **2008**, *18*, 3892.
[16] J. Tersoff, *Appl. Phys. Lett.* **1993**, *62*, 693.
[17] F. Romanato, E. Napolitani, A. Carnera, A. V. Drigo, L. Lazzarini, G. Salviati, C. Ferrari, A. Bosacchi, S. Franchi, *J. Appl. Phys.* **1999**, *86*, 4748.
[18] B. Bertoli, E. N. Suarez, J. E. Ayers, F. C. Jain, *J. Appl. Phys.* **2009**, *106*, 073519.
[19] M. Brazier, M. McElfresh, S. Mansour, *Appl. Phys. Lett.* **1999**, *74*, 299.
[20] N. W. Schubring, J. V. Mantese, A. L. Micheli, A. B. Catalan, R. J. Lopez, *Phys. Rev. Lett.* **1992**, *68*, 1778.
[21] J. V. Mantese, N. W. Schubring, A. L. Micheli, A. B. Catalan, M. S. Mohammed, R. Naik, G. W. Auner, *Appl. Phys. Lett.* **1997**, *71*, 2047.
[22] M. Brazier, M. McElfresh, S. Mansour, *Appl. Phys. Lett.* **1998**, *72*, 1121.
[23] D. Bao, X. Yao, L. Zhang, *Appl. Phys. Lett.* **2000**, *76*, 2779.
[24] N. Choudhury, L. Walizer, S. Lisenkov, L. Bellaiche, *Nature* **2011**, *470*, 513.

© 2013 WILEY-VCH Verlag GmbH & Co. KGaA, Weinheim

[25] G. Catalan, A. Lubk, A. H. G. Vlooswijk, E. Snoeck, C. Magen, A. Janssens, G. Rispens, G. Rijnders, D. H. A. Blank, B. Noheda, *Nat Mater* **2011**, *10*, 963.
[26] D. Lee, A. Yoon, S. Y. Jang, J. G. Yoon, J. S. Chung, M. Kim, J. F. Scott, T. W. Noh, *Phys. Rev. Lett.* **2011**, *107*, 057602.
[27] M. Adachi, Y. Akishige, T. Asahi, K. Deguchi, K. Gesi, K. Hasebe, T. Hikita, T. Ikeda, Y. Iwata, M. Komukae, T. Mitsui, E. Nakamura, N. Nakatani, M. Okuyama, T. Osaka, A. Sakai, E. Sawaguchi, Y. Shiozaki, T. Takenaka, K. Toyoda, T. Tsukamoto, T. Yagi, in *Landolt-Börnstein - Group III Condensed Matter*, Vol. *36A1* (Eds: Y. Shiozaki, E. Nakamura, T. Mitsui), Springer, Berlin, Heidelberg **2001**, p. 16.
[28] K. Boldyreva, L. Pintilie, A. Lotnyk, I. B. Misirlioglu, M. Alexe, D. Hesse, *Ferroelectrics* **2008**, *370*, 140.
[29] P. Williams, *Ann. Rev. Mater. Sci.* **1985**, *15*, 517.
[30] V. Nagarajan, I. G. Jenkins, S. P. Alpay, H. Li, S. Aggarwal, L. Salamanca-Riba, A. L. Roytburd, R. Ramesh, *J. Appl. Phys.* **1999**, *86*, 595.
[31] N. A. Pertsev, A. G. Zembilgotov, *J. Appl. Phys.* **1996**, *80*, 6401.
[32] J. Karthik, A. R. Damodaran, L. W. Martin, *Phys. Rev. Lett.* **2012**, *108*, 167601.
[33] R. Mahjoub, S. P. Alpay, V. Nagarajan, *Phys. Rev. Lett.* **2010**, *105*, 197601.
[34] J. Karthik, A. R. Damodaran, L. W. Martin, *Adv. Mater.* **2012**, *24*, 1610.
[35] B. H. Park, T. W. Noh, J. Lee, C. Y. Kim, W. Jo, *Appl. Phys. Lett.* **1997**, *70*, 1101.
[36] W. L. Warren, B. A. Tuttle, D. Dimos, G. E. Pike, H. N. Al-Shareef, R. Ramesh, J. T. Evans, *Jpn. J. Appl. Phys.* **1996**, *35*, 1521.
[37] L. Pálová, P. Chandra, K. M. Rabe, *Phys. Rev. B* **2007**, *76*, 014112.
[38] G. Catalan, L. J. Sinnamon, J. M. Gregg, *J. Phys.: Condens. Matter* **2004**, *16*, 2253.
[39] G. Catalan, B. Noheda, J. McAneney, L. J. Sinnamon, J. M. Gregg, *Phys. Rev. B* **2005**, *72*, 020102.
[40] I. Vrejoiu, G. Le Rhun, L. Pintilie, D. Hesse, M. Alexe, U. Gösele, *Adv. Mater.* **2006**, *18*, 1657.

© 2013 WILEY-VCH Verlag GmbH & Co. KGaA, Weinheim